



Engineering arbitrarily oriented spatiotemporal optical vortices using transmission nodal lines

HAIWEN WANG,¹ CHENG GUO,¹ WEILIANG JIN,² ALEX Y. SONG,² AND SHANHUI FAN^{2,*}

¹Department of Applied Physics, Ginzton Laboratory, Stanford University, Stanford, California 94305, USA

²Department of Electrical Engineering, Ginzton Laboratory, Stanford University, Stanford, California 94305, USA

*Corresponding author: shanhui@stanford.edu

Received 30 March 2021; revised 23 May 2021; accepted 26 May 2021 (Doc. ID 426460); published 25 June 2021

It has been recently demonstrated that optical pulses can hold transverse orbital angular momentum (OAM). Generation of such vortices typically requires bulky optics, and only OAMs that are fully longitudinal or transverse have been demonstrated until now. Here we investigate a general family of spatiotemporal vortices with arbitrarily oriented OAM and introduce a compact device for its generation. The device operates by having a transmission nodal line, which is a topological defect in the wavevector-frequency spectra of the transmission coefficient. We show that the position and dispersion of the transmission nodal line can be controlled by structural symmetry of the device. By transmitting a Gaussian pulse through the device, we can generate spatiotemporal vortices with its nodal line and OAM oriented along any arbitrary direction. This ability to generate a full family of spatiotemporal vortex pulses may find application in pulse shaping or sensing in the spatiotemporal domain. Our work also provides a novel approach of engineering topological response functions in photonic crystal slabs. © 2021 Optical Society of America under the terms of the [OSA Open Access Publishing Agreement](#)

<https://doi.org/10.1364/OPTICA.426460>

1. INTRODUCTION

Optical vortices are electromagnetic wave configurations that carry phase winding around nodal lines in their field distributions in real space time (Fig. 1). A prominent example of optical vortices are beams or pulses that carry longitudinal orbital angular momentum (OAM) [Fig. 1(b)], where the nodal line is parallel to the direction of propagation [1]. Optical beams or pulses that carry longitudinal OAM have been used in applications such as optical trapping [2,3], super-resolution imaging [4,5], optical communication [6,7], and quantum key distribution [8].

In addition to beams and pulses that carry longitudinal OAM, there are emerging interests in studying other nodal line configurations [9–11]. In particular, recent works have demonstrated optical pulses that carry transverse OAM [12,13], which possesses a nodal line perpendicular to the direction of propagation [Fig. 1(c)]. At present, generating such transverse OAM requires sophisticated optical systems that perform wavefront and spectral shaping. To facilitate further studies of optical vortices, it is important to develop alternative ways for generation of optical vortices that are compact and versatile.

In this paper, we show that an optical pulse with a nodal line in real space time can in general be created by passing a standard Gaussian pulse through a photonic crystal slab structure that possesses a corresponding nodal line structure in its transmission function $t(k_x, k_y, \omega)$ [Fig. 1(e)]. Here ω denotes the frequency. The pulse is assumed to be propagating along the z direction. k_x and k_y are wavevector components in the $x - y$ plane perpendicular to the z axis. As an illustration we introduce photonic

crystal slab structures for the generation of a pulse with transverse OAM, as well as OAM with arbitrary orientations with respect to the propagation direction. Our work points to the significant opportunities for designing nanophotonic structures in the control of optical vortices, and it also highlights the important conceptual connection between the topology of electromagnetic fields in real space and time as well as the topology of the response function in the reciprocal space of wavevector and frequency.

2. OPTICAL VORTICES AND TRANSMISSION NODAL LINES

We consider a optical pulse with a nodal line in real space time (x, y, t) . We assume the pulse has a uniform polarization, so its amplitude can be described by a complex scalar E . At a given plane of constant z , the field is assumed to be

$$E(x, y, t) = (A_x x + A_y y \sin \alpha + A_z c t \cos \alpha) \times \exp\left(-\frac{\Delta\omega^2 t^2}{4} - \frac{\Delta k_x^2 x^2}{4} - \frac{\Delta k_y^2 y^2}{4}\right). \quad (1)$$

Here c is the speed of light; $\Delta\omega$, Δk_x , and Δk_y are widths in frequency and wavevectors of the pulse. We assume A_y is real and A_x is complex with a nonzero imaginary part. Therefore, the nodal line lies in the $y - t$ plane with $x = 0$, and has a 2π phase winding around it. α is the angle of the nodal line relative to the y axis, and it takes value in $(-\pi/2, \pi/2]$. We note that with proper choice of

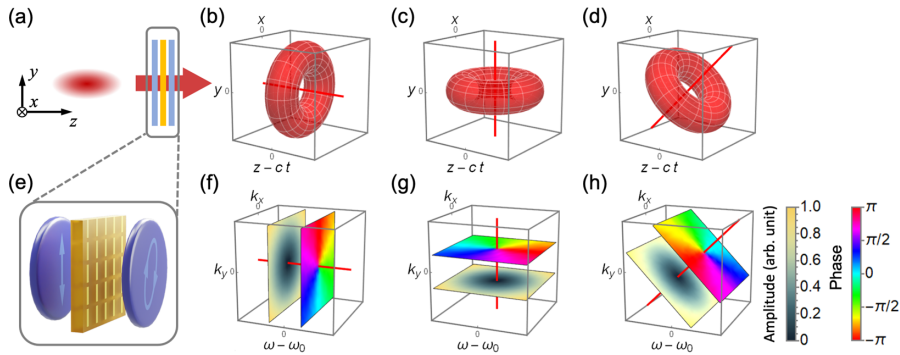


Fig. 1. Schematic of spatiotemporal vortices and its generation method. (a) Input Gaussian pulse. (b)–(d) Various spatiotemporal vortices. The torus shows its iso-intensity surface, and its nodal line in real space time is shown with the red line. All pulses propagate along z . (b) Conventional vortex pulse carrying longitudinal OAM. (c) Pulse carrying transverse vortex and transverse OAM. (d) Pulse with its vortex and OAM pointing at an arbitrary direction. (e) Device for generating the transmission function shown in (f)–(h). It consists of two polarizers (which can itself be a combination of linear polarizers and wave plates, colored in blue) and a photonic crystal slab in the middle (colored in yellow). (f)–(h) The transmission function $t(k_x, k_y, \omega)$ needed to transform a Gaussian pulse into the corresponding spatiotemporal vortex in each column. One slice represents its amplitude, and another slice represents phase.

the coordinate system, Eq. (1) can be used to describe a nodal line with arbitrary orientation.

To see how such pulse can be generated, we transform the field in Eq. (1) into the Fourier domain:

$$E(k_x, k_y, \omega) = N(C_x k_x + C_y k_y \sin \beta - C_y \frac{\omega - \omega_0}{c} \cos \beta) \times \exp \left[-\frac{(\omega - \omega_0)^2}{\Delta \omega^2} - \frac{k_x^2}{\Delta k_x^2} - \frac{k_y^2}{\Delta k_y^2} \right]. \quad (2)$$

We have used the $e^{i\omega t - ik \cdot r}$ convention. ω_0 is the carrier frequency of the pulse. $N = \frac{4\sqrt{2}i}{\Delta \omega \Delta k_x \Delta k_y}$. The parameters C_x , C_y , and β are given by

$$C_x = \frac{A_x}{\Delta k_x^2}, \quad (3)$$

$$C_y = A_y \sqrt{\left(\frac{\sin \alpha}{\Delta k_y^2} \right)^2 + \left(\frac{c^2 \cos \alpha}{\Delta \omega^2} \right)^2}, \quad (4)$$

$$\tan \beta = \frac{\Delta \omega^2}{\Delta k_y^2 c^2} \tan \alpha. \quad (5)$$

We see here that C_y is real and C_x is complex with a nonzero imaginary part. β characterizes the orientation of the nodal line of the pulse in the wavevector-frequency space. From the Fourier space representation of the spatiotemporal vortex, we see that such vortex can be generated by passing a Gaussian pulse through a system S that has a transmission function

$$t_S(k_x, k_y, \omega) \propto C_x k_x + C_y k_y \sin \beta - C_y \frac{\omega - \omega_0}{c} \cos \beta \quad (6)$$

in the lowest order of Taylor expansion. See Fig. 1(a) for a schematic of such generation process. This transmission function has a *transmission nodal line* in the frequency-wavevector space, with a *nodal line dispersion* $\omega_{NL} = \omega_0 + ck_y \tan \beta$. Around the transmission nodal line there is a 2π phase winding.

In Eq. (1), a pulse with a longitudinal OAM has $\alpha = \pi/2$ [Fig. 1(b)]. To generate such a pulse by transmission through an optical system, based on Eq. (5), we see $\beta = \pi/2$. The desired

transmission function contains a vortex in the $k_x - k_y$ plane, and it is independent of frequency [Fig. 1(f)]. Such transmission function is recently realized experimentally [14]. Also in Eq. (1), a pulse with a purely transverse OAM has $\alpha = 0$ [Fig. 1(c)]. From Eq. (5) we have $\beta = 0$. The transmission function thus exhibits a vortex in the $\omega - k_x$ plane, and it is independent of k_y [Fig. 1(g)]. In general, to generate a pulse with nodal line oriented along an arbitrary direction as characterized by the angle α , there is a unique β in $(-\pi/2, \pi/2]$ that satisfies Eq. (5). Therefore, we simply need to design a transmission function with the prescribed β . A schematic of the pulse and corresponding transmission function is shown in Figs. 1(d) and 1(h). As an additional note, an arbitrarily oriented nodal line also gives rise to arbitrarily oriented orbital angular momentum \mathbf{L} . For the pulse in Eq. (1), \mathbf{L} lies in the $y - z$ plane, and its angle γ with respect to the y axis is given by

$$\tan \gamma = \frac{L_z}{L_y} = \frac{(\Delta k_x^2 + \Delta k_y^2) \Delta \omega^2 / c^2}{(\Delta k_x^2 + \Delta \omega^2 / c^2) \Delta k_y^2} \tan \alpha. \quad (7)$$

Detailed derivation of Eq. (7) is provided in [Supplement 1](#).

Our work differs from [15–18], which also investigates nodal lines in light field. Here we consider a polychromatic field forming a pulse in time and the nodal line is propagating with the pulse, whereas these previous works involve monochromatic field and the nodal line is stationary in space. Our nodal line exists in $(2+1)$ D space time (x, y, t), while in these previous works the nodal line exists in 3D space (x, y, z).

3. DESIGNING TRANSMISSION NODAL LINES IN PHOTONIC CRYSTAL SLAB DEVICES

Now we demonstrate how the transmission function in Eq. (6) can be realized and how its nodal line dispersion can be controlled. We start with a geometric argument to show that nodal lines are generic features of a complex function in three dimensions, such as the transmission function $t_S(k_x, k_y, \omega)$ here. A nodal line of t_S simultaneously satisfies the equations $\text{Re}(t_S) = 0$ and $\text{Im}(t_S) = 0$. Each equation is a surface in the three-dimensional $k_x - k_y - \omega$ space, and the intersection of these two surfaces is generically a line. Such nodal line generically has a nontrivial phase winding around it. This can be seen by locally expanding t_S around its zero.

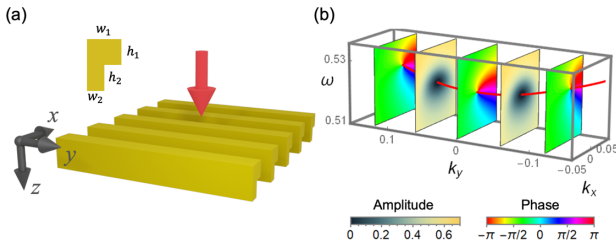


Fig. 2. Photonic crystal slab design for generating pulses with transverse OAM. (a) The geometry of the photonic crystal slab, with incident pulse indicated by the red arrow. The yellow part represents material with permittivity $\epsilon = 12$. The grating cross section in the $x - z$ plane is shown on the top left inset. The dimensions are $w_1 = 0.4a$, $w_2 = 0.2a$, $h_1 = 0.3a$, and $h_2 = 0.3a$, where a is the periodicity. (b) The transmission function of the photonic crystal slab for y -polarized input and output waves. Slices are taken at $k_y = -0.12, 0.0, 0.12$ for phase and $k_y = \pm 0.06$ for amplitude. The red line represents the transmission nodal line. ω and k_x , k_y are in units of $2\pi c/a$ and $2\pi/a$, respectively.

We realize the transmission function $t_S(k_x, k_y, \omega)$ using polarization selected transmission through a photonic crystal slab as illustrated in Fig. 1(e). In this setup, we send a pulse with a uniform polarization, as described by a Jones vector $|E_{\text{in}}\rangle$, into the photonic crystal slab. The pulse transmitted through the slab is then passed through a polarizer selecting an output polarization as described by a Jones vector $|E_{\text{out}}\rangle$. The transmission of a photonic crystal slab can be described by a Jones matrix $J(k_x, k_y, \omega)$. The transmission function of this setup is then [19,20]

$$t_S(k_x, k_y, \omega) = \langle E_{\text{out}} | J(k_x, k_y, \omega) | E_{\text{in}} \rangle. \quad (8)$$

To design a transmission nodal line, the first step is to achieve a zero at a particular transverse wavevector and frequency $(k_{x0}, k_{y0}, \omega_0)$. The plane wave at this transverse wavevector and frequency will have polarization $J(k_{x0}, k_{y0}, \omega_0) |E_{\text{in}}\rangle$ after passing through the photonic crystal slab. We can now choose the output polarizer, selecting a polarization orthogonal to $J(k_{x0}, k_{y0}, \omega_0) |E_{\text{in}}\rangle$, such that this plane wave does not pass through the system. This is known as the cross-polarization condition [14]. Once we achieve $t_S(k_{x0}, k_{y0}, \omega_0) = 0$, by the geometric argument above, we expect that there is a nodal line of t_S that passes through $(k_{x0}, k_{y0}, \omega_0)$. This method allows us to create a transmission nodal line anywhere in the (k_x, k_y, ω) space. We provide a numerical demonstration of such construction in [Supplement 1](#).

To gain more control over the orientation of the transmission nodal line, we exploit symmetries in the photonic crystal slab. This allows us to design transmission nodal lines that lie on high symmetry planes of the system. In the rest of the paper, we discuss two designs with different symmetries that controls the nodal line orientation in different ways.

In our first example, we aim to generate a transmission nodal line along the k_y axis. This can produce a pulse with a transverse OAM. The transmission function can be achieved by using a grating structure which is periodic in the x direction with periodicity a as shown in Fig. 2(a). The input and output polarizer are both chosen to be selecting y -polarized light for transmission. We simulate the transmission coefficients of this configuration [21] and plot the slices of the function $t_S(k_x, k_y, \omega)$ in Fig. 2(b). We see the existence of a nodal line that is symmetric in k_y , so at Γ point ($k_x = 0, k_y = 0$) the nodal line is exactly along the k_y direction.

There are three main considerations behind this design. First, for normal incidence, the transmission through the photonic

crystal slab has a zero at some frequency ω_0 . Such zero is guaranteed by the property of a guided resonance at Γ [22]. By the geometric argument above, this allows the existence of a nodal line passing through $(k_x = 0, k_y = 0, \omega_0)$. Second, we have chosen a structure with $y = 0$ mirror plane. This mirror plane symmetry constrains the transmission function. Here the input and output polarizations are both along y , and a mirror operation (M_y) with respect to the $y = 0$ plane results in

$$M_y |E_{\text{in(out)}}\rangle = -|E_{\text{in(out)}}\rangle, \quad (9)$$

$$M_y J(k_x, k_y, \omega) M_y = J(k_x, -k_y, \omega). \quad (10)$$

Here Eq. (10) holds since the $y = 0$ plane is a mirror plane of the structure. Using these relations we get

$$t_S(k_x, k_y, \omega) = t_S(k_x, -k_y, \omega). \quad (11)$$

This symmetry allows the zeros in transmission to be symmetric in k_y . Thus, near the Γ point, the line of zero transmission can be either perpendicular or parallel to the $k_y = 0$ plane. To constrain the nodal line to be along the k_y direction, we need to ensure that there is no zero in the transmission function for $k_y = 0$ and $k_x \neq 0$. This leads us to the third consideration: the cross section choice of the grating structure [Fig. 2(a), inset]. We know that the guided resonances in gratings and photonic crystal slabs have Fano line shape in their transmission spectra [23]. It was shown that for gratings with cross sections being symmetric in either x or z , the guided resonances at $k_x \neq 0$ are guaranteed to have zeros in their transmission spectrum as part of the Fano line shape [24]. Therefore, we choose a grating cross section where neither x nor z mirror symmetry exists [Inset of Fig. 2(a)]. With these considerations, we indeed achieve a nodal line oriented along k_y near the Γ point as already shown in Fig. 2(b). Away from Γ , the transmission nodal line curves away from any high symmetry plane but still remains symmetric about k_y .

To demonstrate the generation of a pulse with transverse OAM using the structure in Fig. 2(a), we consider an incident Gaussian pulse toward the system in the normal direction. We choose $\Delta\omega = 1.5 \times 10^{-4} \cdot 2\pi c/a$ and $\Delta k_x = \Delta k_y = 1 \times 10^{-3} \cdot 2\pi/a$, and $\omega_0 = 0.52200 \times 2\pi c/a$. The choices of parameters can be quite arbitrary, except that the center wavevector and frequency should be aligned with the zero in transmission at Γ . For larger Δk and $\Delta\omega$, we expect more distortions in the pulse, since the lowest order Taylor expansion of Eq. (6) is no longer accurate. The field envelope and phase are shown in Fig. 3 at different cross sections. Combining the images in Figs. 3(a) and 3(b), we see that the field on the $x - t$ plane has a doughnut-shaped amplitude distribution with phase singularity at the center. In Figs. 3(c) and 3(d), the field on the $y - t$ plane shows that the nodal line lies along the y direction, and the phase variation across the nodal line is π . We numerically calculate the OAM carried by this pulse. The values are $(L_x, L_y, L_z) = (0.00, 3.39, 0.00)\hbar$ per photon. This indicates that our device can indeed generate pulses carrying transverse OAM. The angular momentum value here is not quantized to integers of \hbar because the pulse here, if a snapshot is taken at given time, is not cylindrically symmetric in the $x - z$ plane. Therefore, the field contains “higher-order harmonics” in the form $\exp(il\theta)$, where l is an integer larger than 1 and θ is the angle in the $x - z$ plane. This leads to a nonquantized value of OAM. Detailed calculation and discussion of OAM are in [Supplement 1](#).

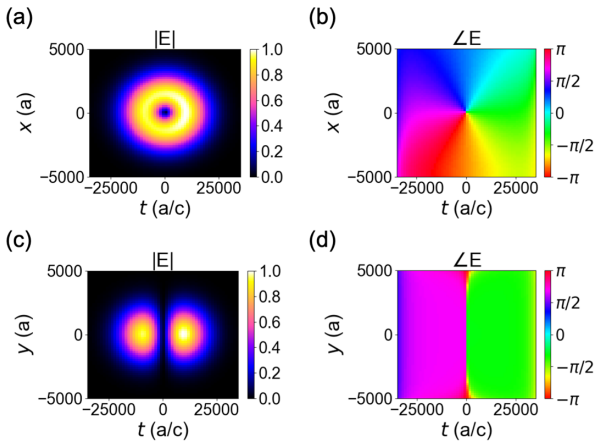


Fig. 3. Numerical simulation of the pulse transmitted through the structure in Fig. 2(a). (a) Amplitude and (b) phase for the pulse envelope at $y = 0$. (c) Amplitude and (d) phase for the pulse envelope at $x = 0$. The nodal line lies parallel with the y axis, through $x = 0$. Amplitudes are normalized to the maximum value in the pulse.

This design can generate not only pulses with transverse OAM but also pulses with OAM along a tilted direction. This can be achieved by tilting the photonic crystal slab about the x and y axes. In this case, a pulse propagating along z is incident upon the photonic crystal slab at an oblique angle. The nodal line dispersion probed by the input pulse, represented by β , is neither 0 nor $\pi/2$. However, because the nodal line moves away from the $k_x = 0$ plane away from the Γ point, we have to control two tilting angles of the photonic crystal slab to find the operating point. To reduce the complexity of the control required in order to generate OAM along an arbitrary tilted direction, in our second design, we aim to find a configuration where the entire nodal line is pinned on a high symmetry plane. In this case, controlling a single tilting angle of the photonic crystal slab allows us to move the operation point along the nodal line, to generate a pulse with an arbitrary β parameter in Eq. (2).

In our second design we consider a photonic crystal slab that is symmetric in y and z , and choosing the input to be y polarized and the output to be left circularly polarized (LCP). A representative structure is shown in Fig. 4(a). The structural symmetry and polarization choices results in the nodal line of the transmission function being pinned on the $k_y = 0$ plane. The argument is as follows: With the y mirror symmetry, the guided resonances in the slab at $k_x \neq 0$ and $k_y = 0$ can be classified as even and odd modes with respect to the y mirror operation and a y -polarized input only couples to the odd mode. Therefore, this structure at $k_x \neq 0$ and $k_y = 0$ can be described by a two-mode four-port coupled mode model [25], with the two modes being at $\pm k_x$ and the four ports being the plane waves at $\pm k_x$ on either side of the slab. See Supplement 1 for a graphical illustration. Using the z mirror symmetry and reciprocity, we can see that the coupling constants from each of the resonant modes to each of the ports are all equal. In this case, the transmission of y -polarized light through the photonic crystal slab are guaranteed to have zeros in the Fano lineshape. Therefore, we can generate a line of zeros in transmission that is pinned on the $k_y = 0$ plane. To ensure a 2π phase winding around such zero, we choose the output polarization $|E_{out}\rangle$ to be one of the circular polarization, in our case the left circular polarization. This ensures the transmission coefficients has no symmetry with respect to k_y . If we were to choose y or x polarization at the output, the

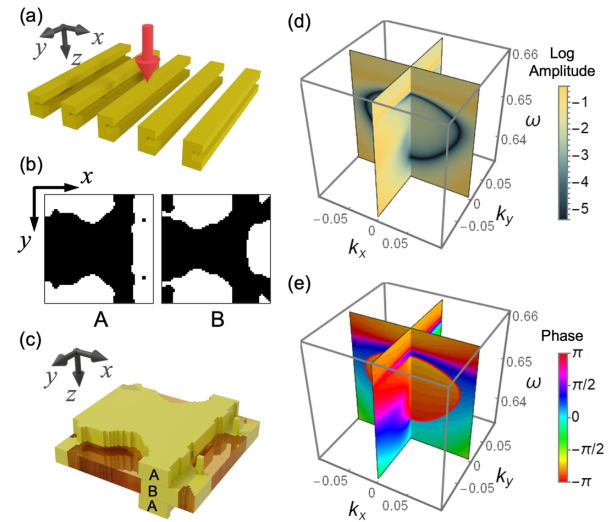


Fig. 4. Photonic crystal slab design for symmetry constrained nodal line. (a) Grating structure with correct symmetry to pin the transmission nodal line on the $k_y = 0$ plane. Normal incident pulse is denoted by the red arrow. (b) Inverse designed dielectric pattern for near isotropic transmission vortex. In layer A, the black part represents $\epsilon = 12$ and the white part represents $\epsilon = 1$. In layer B, the black part represents $\epsilon = 12$ and the white part represents $\epsilon = 2.3$. (c) 3D visualization of inverse designed unit cell, composed of ABA layers. The periodicity is a for both the x and y directions. Layer A has thickness $0.113a$, and layer B has thickness $0.115a$. The thickness is also chosen by the optimization algorithm. (d) Log amplitude of transmission of y -polarized input, LCP output for the structure in (c). We see the zero of the transmission lies on the $k_y = 0$ plane. (e) The phase of the transmission coefficient. The red line represents the nodal line, with a π phase difference on either side.

transmission coefficients would be symmetric or antisymmetric in k_y , which would not result in a 2π phase winding.

In this design, reciprocity guarantees the transmission nodal line to be symmetric in k_x . To see this, notice that for y -polarized plane waves with $k_x \neq 0$ and $k_y = 0$, due to the mirror symmetry along y , the plane wave does not go through polarization conversion. It remains polarized in the y direction after transmitting through the photonic crystal slab, before passing through the output polarizer. In this case of $k_y = 0$, the output polarizer modifies the transmission coefficient by a constant factor that is independent of k_x in the paraxial limit. Using reciprocity together with z mirror symmetry, we see $t_S(k_x, k_y = 0, \omega) = t_S(-k_x, k_y = 0, \omega)$. Thus, the transmission nodal line, which lies in the $k_y = 0$ plane, is symmetric in k_x .

The symmetry and reciprocity argument above guarantees the existence of a nodal line in the $\omega - k_x$ plane. But the detailed shape of the phase winding around the nodal line depends on the details of the structure. We numerically calculate the transmission coefficients of the grating structure in Fig. 4(a). Its transmission nodal line lies on the $k_y = 0$ plane, but the phase winding around it is very anisotropic. The results are shown in Supplement 1. To generate a more isotropic vortex, we use a topology optimization method [21] that maintains z mirror and y mirror symmetry throughout the optimization process. (The details of the optimization method are found in Supplement 1.) An optimized structure is shown in Fig. 4(b) for in-plane patterns of a unit cell and in Fig. 4(c) for a 3D rendered unit cell. The structure shown here is a output of the optimization algorithm with a particularly choice of initial

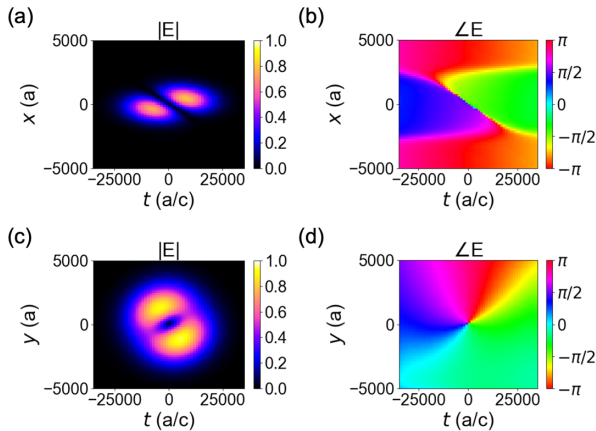


Fig. 5. Numerical simulation of pulse transmitted from the structure in Fig. 4(c). (a) Amplitude and (b) phase for the pulse envelope at $y = 0$. The nodal line of the pulse lies in this plane, indicated by the absence of the vortex in phase. (a) Amplitude and (b) phase for the pulse envelope at $x = 0$. Amplitudes are normalized to the maximum value in the pulse.

structure. The optimized structure can vary with difference choices of the initial structure.

The complex transmission coefficients with y -polarization input and LCP output are shown in Figs. 4(d) and 4(e). We see the nodal line is indeed pinned on the $\omega - k_x$ plane with $k_y = 0$ and forms a nodal ring. The π phase difference of the phase on different side of the nodal line is a strong indication that the nodal line is exactly on the $k_y = 0$ plane. In the $\omega - k_y$ plane, the transmission zeros are isolated points and has 2π phase winding around the zeros.

To generate a pulse with tilted OAM, we choose an input pulse with $\Delta k_x = 2 \times 10^{-3} \cdot 2\pi/a$, $\Delta k_y = 1 \times 10^{-3} \cdot 2\pi/a$, $\Delta\omega = 1.5 \times 10^{-4} \cdot 2\pi c/a$, and $\omega_0 = 0.63902 \times 2\pi c/a$. We rotate the photonic crystal slab around the y axis such that a pulse propagating along the optical axis corresponds to $k_{x'} = 0.02 \times 2\pi/a$ in the coordinate of photonic crystal slab. Around this point, the transmission function of the slab has a tilted nodal line in (k_x, k_y, ω) space, with a dispersion $d\omega/dk_x = c \tan \beta \approx 0.054c$. The parameters of the pulses are chosen so that the pulse probes only a local region around $k_{x'}$ where the lowest order Taylor expansion of Eq. (6) is valid. According to Eq. (5), the output pulse will be a spatiotemporal vortex, with its nodal line tilted $\alpha = 84.1^\circ$ relative to the x axis, in the $x - z$ plane. This is verified by numerical calculation of the output pulse, shown in Fig. 5. In Figs. 5(a) and 5(b), we see the nodal line lies completely in $x - t$ plane, and the extracted slope of the nodal line is $0.11c$, which agrees well with the prediction $\cot \alpha = 0.10$. The $y - t$ plane cross section of the simulated pulse is shown in Figs. 5(c) and 5(d). We clearly see that it contains a vortex. The orbital angular momentum for this pulse is $(L_x, L_y, L_z) = (2.38, -0.001, 0.61)\hbar$ per photon. The orientation of \mathbf{L} is characterized by $\gamma = 14^\circ$, which agrees well with Eq. (7).

4. DISCUSSION AND CONCLUSION

In our second example, the nodal line forms a loop. Therefore, for any nodal line orientation α in Eq. (1), there exist an orientation of the photonic crystal slab that can be used to generate pulse with such nodal line orientation. This allows us to continuously tune

the nodal line and the OAM of the pulse, from being longitudinal to transverse, and also along any arbitrary direction. In addition, we can rotate the whole device around the z axis to achieve any azimuthal angle we want for the nodal line and OAM. Therefore, our design is general for generating an entire family of spatiotemporal optical vortices carrying OAM. Our device is much more compact than what was used in [12,13] to generate a transverse OAM.

Throughout the paper, we assumed paraxial fields. In the case where such approximation breaks down, a longitudinal field component arises and may lead to various spin-orbit coupling phenomena [26,27]. The vortices we demonstrated have unity charge. Higher-order topological charges can be designed using compact photonic structure in principle. Alternatively, we can also achieve higher-order charges by cascading the device proposed here.

We briefly discuss the experimental considerations of the proposed scheme. In all our calculations above, we considered a Gaussian pulse that is both transversely and longitudinally at focus, at the position of the device. However, our device in fact can be placed at any longitudinal position before or after the focus, since both our device and vacuum propagation conserves the transverse momentum [28]. The demonstrated pulse dimensions, in both transverse and longitudinal directions, are similar to what has been demonstrated experimentally [12–14], and the interferometric approach in [12–14] can be used to reveal the phase structure of the pulse. Our method requires alignment of the pulse central frequency to the frequency of the transmission nodal line. This alignment is experimentally achievable [29]. For fabrication of the device, the main concern may be the smallest feature size in the structure obtained by inverse design. One may address this concern by imposing a constraint on the minimum feature size in the inverse design algorithm [30,31].

In conclusion, we investigated properties of spatiotemporal optical vortex pulses carrying nodal line along arbitrary directions and showed that it carries OAM along an arbitrary orientation with respect to its propagation direction. We show that such vortex pulses can be generated by using polarization selected transmission of photonic crystal slabs that host transmission nodal lines in 3D wavevector-frequency space. By having different symmetries in the photonic crystal slab, the direction of such transmission nodal line can be pinned to be along some high symmetry direction or high symmetry plane, which simplifies the control that is required to generate spatiotemporal optical vortex pulses. Our design is much more compact and more versatile than previous realizations that generate transverse OAM. This device represents an important step forward in advancing fundamental studies and practical applications of spatiotemporal optical vortex pulses.

Funding. Office of Naval Research (N00014-20-1-2450).

Acknowledgment. The authors thank Charles C. Wojcik and Tengfeng Zhu for helpful discussions.

Disclosures. The authors declare no conflicts of interest.

Data availability. Data underlying the results presented in this paper are not publicly available at this time but may be obtained from the authors upon reasonable request.

Supplemental document. See Supplement 1 for supporting content.

REFERENCES

1. Y. Shen, X. Wang, Z. Xie, C. Min, X. Fu, Q. Liu, M. Gong, and X. Yuan, "Optical vortices 30 years on: OAM manipulation from topological charge to multiple singularities," *Light Sci. Appl.* **8**, 1–29 (2019).
2. L. Paterson, M. P. MacDonald, J. Arlt, W. Sibbett, P. Bryant, and K. Dholakia, "Controlled rotation of optically trapped microscopic particles," *Science* **292**, 912–914 (2001).
3. M. Padgett and R. Bowman, "Tweezers with a twist," *Nat. Photonics* **5**, 343–348 (2011).
4. F. Tamburini, G. Anzolin, G. Umbriaco, A. Bianchini, and C. Barbieri, "Overcoming the Rayleigh criterion limit with optical vortices," *Phys. Rev. Lett.* **97**, 163903 (2006).
5. L. Yan, P. Gregg, E. Karimi, A. Rubano, L. Marrucci, R. Boyd, and S. Ramachandran, "Q-plate enabled spectrally diverse orbital-angular-momentum conversion for stimulated emission depletion microscopy," *Optica* **2**, 900–903 (2015).
6. J. Wang, J.-Y. Yang, I. M. Fazal, N. Ahmed, Y. Yan, H. Huang, Y. Ren, Y. Yue, S. Dolinar, M. Tur, and A. E. Willner, "Terabit free-space data transmission employing orbital angular momentum multiplexing," *Nat. Photonics* **6**, 488–496 (2012).
7. N. Bozinovic, Y. Yue, Y. Ren, M. Tur, P. Kristensen, H. Huang, A. E. Willner, and S. Ramachandran, "Terabit-scale orbital angular momentum mode division multiplexing in fibers," *Science* **340**, 1545–1548 (2014).
8. G. Vallone, V. D'Ambrosio, A. Sponselli, S. Slussarenko, L. Marrucci, F. Sciarrino, and P. Villoresi, "Free-space quantum key distribution by rotation-invariant twisted photons," *Phys. Rev. Lett.* **113**, 060503 (2014).
9. J. F. Nye and M. V. Berry, "Dislocations in wave trains," *Proc. R. Soc. London A* **336**, 165–190 (1974).
10. A. Sukhorukov and V. Yangirova, "Spatio-temporal vortices: properties, generation and recording," *Proc. SPIE* **5949**, 594906 (2005).
11. K. Y. Bliokh and F. Nori, "Spatiotemporal vortex beams and angular momentum," *Phys. Rev. A* **86**, 033824 (2012).
12. S. Hancock, S. Zahedpour, A. Goffin, and H. Milchberg, "Free-space propagation of spatiotemporal optical vortices," *Optica* **6**, 1547–1553 (2019).
13. A. Chong, C. Wan, J. Chen, and Q. Zhan, "Generation of spatiotemporal optical vortices with controllable transverse orbital angular momentum," *Nat. Photonics* **14**, 350–354 (2020).
14. T. Zhu, C. Guo, J. Huang, H. Wang, M. Orenstein, Z. Ruan, and S. Fan, "Topological optical differentiator," *Nat. Commun.* **12**, 680 (2021).
15. J. Leach, M. R. Dennis, J. Courtial, and M. J. Padgett, "Knotted threads of darkness," *Nature* **432**, 165 (2004).
16. J. Leach, M. R. Dennis, J. Courtial, and M. J. Padgett, "Vortex knots in light," *New J. Phys.* **7**, 55 (2005).
17. F. Flossmann, U. T. Schwarz, M. Maier, and M. R. Dennis, "Polarization singularities from unfolding an optical vortex through a birefringent crystal," *Phys. Rev. Lett.* **95**, 253901 (2005).
18. A. H. Dorrah, C. Rosales-Guzmán, A. Forbes, and M. Mojahedi, "Evolution of orbital angular momentum in three-dimensional structured light," *Phys. Rev. A* **98**, 043846 (2018).
19. W. Singer, M. Totzeck, and H. Gross, *Handbook of Optical Systems, Volume 2: Physical Image Formation* (Wiley, 2006).
20. Z. Shi, A. Y. Zhu, Z. Li, Y.-W. Huang, W. T. Chen, C.-W. Qiu, and F. Capasso, "Continuous angle-tunable birefringence with freeform metasurfaces for arbitrary polarization conversion," *Sci. Adv.* **6**, eaba3367 (2020).
21. W. Jin, W. Li, M. Orenstein, and S. Fan, "Inverse design of lightweight broadband reflector for relativistic lightsail propulsion," *ACS Photon.* **7**, 2350–2355 (2020).
22. K. X. Wang, Z. Yu, S. Sandhu, and S. Fan, "Fundamental bounds on decay rates in asymmetric single-mode optical resonators," *Opt. Lett.* **38**, 100–102 (2013).
23. S. Fan and J. D. Joannopoulos, "Analysis of guided resonances in photonic crystal slabs," *Phys. Rev. B* **65**, 235112 (2002).
24. H. Zhou, B. Zhen, C. W. Hsu, O. D. Miller, S. G. Johnson, J. D. Joannopoulos, and M. Soljačić, "Perfect single-sided radiation and absorption without mirrors," *Optica* **3**, 1079–1086 (2016).
25. W. Suh, Z. Wang, and S. Fan, "Temporal coupled-mode theory and the presence of non-orthogonal modes in lossless multimode cavities," *IEEE J. Quantum Electron.* **40**, 1511–1518 (2004).
26. K. Y. Bliokh, F. J. Rodríguez-Fortuño, F. Nori, and A. V. Zayats, "Spin-orbit interactions of light," *Nat. Photonics* **9**, 796–808 (2015).
27. K. Y. Bliokh, "Spatiotemporal vortex pulses: angular momenta and spin-orbit interaction," *Phys. Rev. Lett.* (to be published).
28. H. Wang, C. Guo, Z. Zhao, and S. Fan, "Compact incoherent image differentiation with nanophotonic structures," *ACS Photon.* **7**, 338–343 (2020).
29. F. Liu, T. Wang, L. Qiang, T. Ye, Z. Zhang, M. Qiu, and Y. Su, "Compact optical temporal differentiator based on silicon microring resonator," *Opt. Express* **16**, 15880–15886 (2008).
30. L. Su, A. Y. Piggott, N. V. Sapra, J. Petykiewicz, and J. Vuckovic, "Inverse design and demonstration of a compact on-chip narrowband three-channel wavelength demultiplexer," *ACS Photon.* **5**, 301–305 (2018).
31. T. W. Hughes, I. A. Williamson, M. Minkov, and S. Fan, "Forward-mode differentiation of Maxwell's equations," *ACS Photon.* **6**, 3010–3016 (2019).